Published in final edited form as:
Nat Neurosci. 2016 July ; 19(7): 926–934. doi:10.1038/nn.4319.

SHANK3 controls maturation of social reward circuits in the VTA

Sebastiano Bariselli[#1], **Stamatina Tzanoulinou**[#1], **Christelle Glangetas**[1,2,3], **Clément Prévost-Solié**[1], **Luca Pucci**[1], **Joanna Viguié**[4], **Paola Bezzi**[1], **Eoin C. O'Connor**[4], **François Georges**[2,3,6], **Christian Lüscher**[4,5], and **Camilla Bellone**[1]

[1]Dept. of Fundamental Neurosciences, University of Lausanne, CH-1005, Lausanne, Switzerland [2]Centre National de la Recherche Scientifique, Interdisciplinary Institute for Neuroscience, UMR 5297, Bordeaux, France [3]Université de Bordeaux, Bordeaux, France [4]Dept. of Basic Neurosciences, Medical Faculty, University of Geneva, CH-1211 Geneva, Switzerland [5]Clinic of Neurology, Geneva University Hospital, CH-1211 Geneva, Switzerland [6]Centre National de la Recherche Scientifique, Neurodegeneratives diseases Institute, UMR 5293, Bordeaux, France

[#] These authors contributed equally to this work.

Summary

Haploinsufficiency of *SHANK3,* encoding the synapse scaffolding protein SHANK3, leads to a highly penetrant form of Autism Spectrum Disorder (ASD). How *SHANK3* insufficiency affects specific neural circuits and this is related to specific ASD symptoms remains elusive. Here we used shRNA to model *Shank3* insufficiency in the Ventral Tegmental Area (VTA) of mice. We identified dopamine (DA) and GABA cell-type specific changes in excitatory synapse transmission that converge to reduce DA neuron activity and generate behavioral deficits, including impaired social preference. Administration of a positive allosteric modulator of the type 1 metabotropic glutamate receptors (mGluR1) during the first postnatal week restored DA neuron excitatory synapse transmission and rescued the social preference defects, while optogenetic DA neuron stimulation was sufficient to enhance social preference. Collectively, these data reveal the contribution of impaired VTA function to social behaviors and identify mGluR1 modulation during postnatal development as a potential treatment strategy.

To whom correspondence should be addressed, Camilla.Bellone@unil.ch.

Author Contributions All VTA-SHANK3 infections were performed by S.B. *In vitro* electrophysiology experiments were performed by S.B. Behavioral experiments were performed by S.T., with assistance from C.P.S., S.B. and E.C.O'C. S.B. and S.T. performed the statistical analyses for the *in vitro* electrophysiology and the behavioral experiments, and contributed to the statistical analysis of the *in vivo* electrophysiology experiments. *In vivo* recordings were performed by C.G and F.G. Immunohistochemistry was performed by S.B., J.V. and C.G. Western blots were performed by L.P and P.B. The study was designed and the manuscript written by C.B., with assistance from S.B., E.C.O'C, C.L and F.G.

Accession codes

We used the following shRNA sequence that targets exon 21 of the rat and mouse *SHANK3* gene (GenBank™ accession number NM_021423.3): 5′ GGAAGTCACCAGAGGACAAGA-3′

Europe PMC Funders Author Manuscripts

Introduction

Autism spectrum disorders (ASDs) constitute a heterogeneous group of neurodevelopmental conditions characterized by impairments in two core domains: communication and social behavior and repetitive/stereotyped actions1,2. Behavioral interventions for social deficits have been suggested, while current pharmacotherapy is limited to reducing ASD symptoms such as irritability (e.g. risperidone), but fails to address impairments in any of the core domains. To aid the development of new treatment options, a better understanding of how brain circuits controlling social and repetitive behaviors are altered in ASDs is required.

Brain regions involved in the control of social behavior and repetitive actions show a surprising degree of overlap, encompassing corticolimbic-ventral striatal networks3,4. Notably, these regions are subject to modulation by dopamine (DA) neurons of the ventral tegmental area (VTA) and a growing body of literature points to impaired function of this so-called ‘reward circuit’ as contributing to social deficits in ASD5,6. For example, according to the social motivation hypothesis of autism, social interactions would normally occur because they are inherently rewarding, but ASD individuals show a deficit in assigning value to social stimuli resulting in social dysfunction6. Midbrain DA neurons signal motivationally relevant stimuli7,8, and fiber photometry has revealed an increase in VTA DA neuron Ca^{2+} activity during social interactions9. However, how genetic risk factors affect VTA function and the mechanisms by which this affects social behavior has not been explored.

Although the etiology of autism is unclear, twin studies highlight a strong genetic component of the disease10. Many of the genes implicated in ASDs encode for synaptic proteins and, for this reason, autism is considered as a ‘synaptopathy’11. *SHANK3* is one such gene encoding the excitatory synapse scaffolding protein SHANK3, whose loss or mutation is associated with Phelan-McDermid Syndome12 and other isolated ASD cases13,14. Through its different domains, SHANK3 orchestrates the layout of metabotropic and ionotropic glutamate receptors at the synapse15. For example, the PDZ region is responsible for the indirect link of N-methyl-D-aspartate receptors (NMDARs) and α-amino-3-hydroxy-5-methyl-isoxazolepropionic acid receptors (AMPARs), while the proline-rich domain of SHANK3 binds to metabotropic Glutamate Receptor-group I (mGluR-group I) via Homer protein. In mutant mice with disruptions of distinct SHANK3 domains, a variety of electrophysiological and behavioral phenotypes were reported16–20. While such knockout models underscore the importance of *Shank3* deficiency in impairing behavior, how dysfunction in specific brain circuits may contribute to specific behavioral deficits has not been fully resolved.

The peak of *Shank3* gene expression occurs within the first postnatal week and decreases during the second and third weeks, a critical period of development when activity shapes neuronal connectivity and circuit function. We have previously shown that during the first postnatal week in mice, AMPAR transmission onto VTA DA neurons is mainly mediated by GluA2-lacking AMPARs21. Activation of metabotropic Glutamate Receptor 1 (mGluR1) during postnatal development removes these calcium-permeable AMPARs and inserts GluA2-containing receptors. Notably, removal of mGluR1 or exposure to addictive drugs *in*

utero impairs the postnatal maturation of glutamatergic transmission onto VTA DA neurons, resulting in persistent and aberrant expression of GluA2-lacking AMPARs21,22. Given the importance of SHANK3 in orchestrating excitatory synaptic function, we hypothesized that low levels of SHANK3 in the VTA could also impact on the maturation of excitatory synapses in this structure, driving long-lasting synaptic, circuit and behavioral deficits that could contribute to the pathology of ASDs.

Here we use a shRNA to induce early postnatal downregulation of SHANK3 specifically in the VTA. The resulting SHANK3 insufficiency impairs the maturation of excitatory synapses onto both VTA DA and GABA neurons. These synaptic changes are concomitant with reduced *in vivo* burst activity of DA neurons, increased activity of GABA neurons and behavioral deficits including impaired social preference that persists into adulthood. Providing a causal link between altered DA neuron activity and social behavior, we find that systemic treatment with a positive allosteric modulator (PAM) of mGluR1 during the postnatal period of synapse maturation normalizes social deficits into adulthood, owing to a specific rescue of DA neuron excitatory transmission and activity. Moreover, optogenetic activation of VTA DA neurons increases social preference in SHANK3 deficient mice, confirming sufficiency of DA neuron activity to support social interactions.

Results

SHANK3 insufficiency alters VTA excitatory synaptic transmission

To isolate the potential impact on the VTA caused by global SHANK3 deficiency in some ASD cases, we downregulated SHANK323 in the VTA of mice before Postnatal day (P) 6 using stereotaxic injections of Adeno-Associated Virus (AAV) expressing an shRNA that targets the proline rich domain encoding region of *Shank3* mRNA (shShank3), coupled with the ZsGreen reporter (Fig. 1a). Construct expression was evident 9 days after the injection (Supplementary Fig. 1a), persisted when synapses were mature (more than 20 weeks, data not shown) and was restricted to the VTA, where 61.1% of DA neurons (Tyrosine Hydroxylase, TH, positive) and 39.5% of non-DA cells (i.e. non-TH cells) were infected (Supplementary Fig. 1b). To better quantify the proportion of VTA GABA cells infected, GAD-Cre mice were injected with AAV-DIO-tdTomato (P14) allowing the specific identification of GABA neurons (Fig. 1b). Quantification of ZsGreen expression in TH and tdTomato labeled cells confirmed shShank3 expression in 53.5% of DA neurons and 31.4% of GABA neurons, respectively (Fig. 1b). Western-blot analysis of the VTA, dissected at adolescence, showed a significant decrease in SHANK3 expression in AAV-shShank3 mice compared to animals infected with a scrambled sequence (AAV-scrShank3; Fig. 1c). No difference in SHANK3 expression was found in the neighboring Substantia Nigra (SN; Fig. 1c), indicating that our manipulation was selective for the VTA. Although we did not examine whether morphological changes occurred in VTA neurons, the number of TH positive cells did not differ when comparing AAV-shShank3 infected and Uninfected side in the same animal (Supplementary Fig. 1c), suggesting that shShank3 expression was not affecting cell survival.

Since SHANK3 is enriched in the postsynaptic density of excitatory synapses15, we examined whether early postnatal *Shank3* downregulation in the VTA could give rise to

alterations in excitatory synaptic transmission onto VTA neurons. Whole cell *in vitro* patch clamp recordings from shShank3 or scrShank3 infected cells were performed and Excitatory Post-Synaptic Currents (EPSCs) pharmacologically isolated. We recorded from Putative DA neurons identified by their high capacitance, low input resistance (Supplementary Fig. 2a,b), presence of I_h current and morphology. Recordings were made when the postnatal maturation of VTA DA neuron synapses is normally complete (P18-35; early adolescence)21. Putative DA neurons infected with shShank3 exhibited a higher AMPA/NMDA ratio compared to scrShank3 or Uninfected neurons (Fig. 2a). There was no change in the paired pulse ratio (PPR), pointing to a postsynaptic locus of this effect (Fig. 2b). All together our data indicate that VTA-SHANK3 insufficiency alters glutamatergic transmission onto Putative DA neurons.

At VTA DA neuron synapses, an aberrant increase in the AMPA/NMDA ratio often reflects functional changes in the AMPAR subunit arrangement24,25. To analyze the AMPAR subunit composition, AMPAR-mediated EPSCs were pharmacologically isolated and the Rectification Index (RI) calculated as the slope of the line between current measured at negative and reversal potentials, divided by the corresponding slope measured at positive potentials26. An increase in RI was observed in shShank3 infected Putative DA neurons compared to both scrShank3 and Uninfected Putative DA cells (Fig. 2c). Changes in AMPAR can occur together with changes in NMDAR subunit composition21. However, no change in sensitivity to the GluN2B antagonist ifenprodil or decay time kinetics were found in shShank3 infected vs. Uninfected cells (Fig. 2d-f), indicating that the content of GluN2B/GluN2A containing NMDARs was not affected by SHANK3 insufficiency. Collectively, these data reveal the presence of GluA2-lacking AMPARs at excitatory synapses onto VTA Putative DA neurons of adolescent mice, with no change in NMDAR subunit composition following early postnatal VTA-SHANK3 insufficiency.

How does VTA-SHANK3 insufficiency alter excitatory transmission? In VTA DA neurons, GluA2-lacking AMPARs contribute to synaptic transmission at birth and are then exchanged for GluA2-containing AMPARs during postnatal synapse maturation21. One possibility is that SHANK3 insufficiency prevents this physiological maturation of DA neuron synapses. Alternatively, SHANK3 downregulation alters synaptic transmission irrespective of any developmental influence. To distinguish between these two scenarios, we used AAV-Shank3 into the VTA, but injections were now made after the postnatal period of synapse maturation21 (Fig. 2g). Surprisingly, when SHANK3 was downregulated in the VTA after P20-24, excitatory transmission recorded at P31-P45 remained unaltered (Fig. 2g,h). These data suggest that SHANK3 is required for the maturation of excitatory transmission of VTA DA neurons and once maturation is completed, basal synaptic transmission becomes independent of SHANK3.

We next examined whether postnatal SHANK3 insufficiency affects excitatory transmission onto VTA GABA neurons. Putative GABA neurons were identified by their low capacitance, high input resistance (Supplementary Fig. 2a,b), absence of I_h and characteristic morphology. The AMPA/NMDA ratio was higher in shShank3 infected Putative GABA neurons compared to Uninfected cells, while RI and PPR did not differ (Fig. 3a-c). Thus, VTA-SHANK3 insufficiency also alters glutamatergic transmission onto VTA Putative

GABA neurons but, in contrast to Putative DA neurons, this manipulation does not affect the content of GluA2-containing AMPARs at these synapses where the presence of these receptors has never been investigated during development. Importantly, these data point to cell-type specific functions of SHANK3 within the VTA.

SHANK3 insufficiency alters VTA neuron activity

In the VTA, pharmacological activation of mGluR1 onto DA neurons promotes the switch from GluA2-lacking to GluA2-containing AMPARs[24,26]. We first asked whether this approach could also recover the delayed maturation observed with SHANK3 insufficiency. We monitored AMPAR-EPSCs in VTA Putative DA neurons from adolescent mice infected before P6 and bath applied the group I mGluR agonist DHPG (20 μM). This led to a long-term depression and rendered the current-voltage relationship of AMPAR-transmission linear (Fig. 4a,b).

No long-term changes in AMPAR-mediated transmission or RI were observed after DHPG application in Uninfected Putative DA cells (Fig. 4a,b). Interestingly, DHPG induced a transient short-term depression in both shShank3 and Uninfected cells, which likely reflects release of endocannabinoids, as previously described[27] (Fig. 4a). In VTA GABA Putative neurons, DHPG treatment did not induce long-lasting changes in AMPAR-EPSCs recorded from shShank3 infected nor Uninfected Putative GABA neurons (Supplementary Fig. 3a). Together, these results show that pharmacological activation of mGluR-I in acute brain slices rescue immature AMPAR-transmission through removal of GluA2-lacking AMPARs in Putative DA but not in Putative GABA neurons.

Would such treatment also be efficient if administered *in vivo?* For this purpose, a positive allosteric modulator (PAM) of mGluR1 (Ro 677476; PAM-mGluR1) was used, which offers several advantages over DHPG including selectivity for mGluR1 and facilitation of existing endogenous activity[28]. The PAM-mGluR1 was administered systemically (4 mg/kg, i.p.) once daily starting from P6 until 24 h before *ex vivo* electrophysiological recordings performed between P18-P33 (Fig. 4c). In PAM-mGluR1 treated shShank3 animals the AMPA/NMDA ratio and RI in VTA Putative DA were no different from vehicle scrShank3 mice but significantly lower compared to shShank3 mice treated with vehicle (Fig. 4c,d). PAM-mGluR1 treatment did not affect baseline transmission onto VTA Putative DA neurons in scrShank3 mice. Consistent with the *in vitro* DHPG data, the AMPA/NMDA ratio recorded at excitatory inputs onto VTA GABA neurons remained elevated following PAM-mGluR1 treatment (Supplementary Fig. 3b). These data indicate that *in vivo* PAM-mGluR1 treatment acts specifically at synaptic inputs onto putative DA neurons to normalize the maturation deficit induced by SHANK3 insufficiency.

SHANK3 insufficiency alters VTA neuron activity

Group I mGluRs regulate the firing pattern of DA neurons both *in vivo* and *in vitro*[29,30]. Insufficiency of SHANK3 might therefore lead to altered VTA neuron activity. We performed *in vivo* single unit recordings in adolescent mice previously injected with AAV-shShank3 virus.

Europe PMC Funders Author Manuscripts

We found that the total fraction of VTA Putative DA31 neurons classified as 'burst-firing' was similar in shShank3 mice and scrShank3 controls (Supplementary Fig. 4a,b, Fig. 5a). However, while baseline firing rate did not significantly differ amongst conditions, within the population of burst-firing neurons, the frequency within burst (bursting rate) was significantly lower in shShank3 mice compared to controls (Fig. 5b-d). Conversely the firing rate of Putative GABA neurons (for identification parameters, see methods) was significantly higher in shShank3 mice compared to scrShank3 controls (Fig. 5e,f). Thus, akin to *in vitro* observations, SHANK3 insufficiency leads to cell-type specific changes in the activity of VTA neurons. Since VTA GABA neurons provide local inhibition to DA neurons32, their increased activity may further reduce DA neuron output.

Was PAM-mGluR1 treatment *in vivo* also sufficient to recover VTA Putative DA neuron activity following SHANK3 insufficiency? As before, following early postnatal VTA injections of AAV-shShank3 or AAV-scrShank3, systemic injections of PAM-mGluR1 were made once daily during the period of synapse maturation. As a result, burst activity of putative DA neurons was not different in shShank3 versus scrShank3 mice (Fig. 5b-d). Taken together, these findings confirm that the activation of mGluR1 during synapse maturation is efficient to rescue the maturation deficits in VTA DA arising from SHANK3 insufficiency.

VTA-SHANK3 insufficiency generates social impairments

Shank3 KO mice exhibit a variety of behavioral deficits, including increased self-grooming and social interaction deficits33,16,18. Since DA neuron activity was shown to encode social interactions9, we hypothesized that VTA-SHANK3 insufficiency may affect behaviors in the social domain.

First we assayed social preference in mice, using a three-chamber social interaction test34. In scrShank3 control mice, social preference was maintained for the entire duration of the 10-minute test (Fig. 6a-c). In contrast, in shShank3 mice social preference significantly declined after 5 minutes (T_2 versus T_1, Fig. 6c,d), suggesting a time-dependent loss of social interest. Further analysis showed that reduced social preference could be explained by a shorter social interaction time and a trend toward decreased number of entries (Fig. 6e,f) at the expense of a longer object interaction time during the second half of the observation period T_2 (Supplementary Fig. 5c). These effects were not observed in T1 (Supplementary Fig. 5a,b). Impaired social preference was also observed in mice injected with a smaller volume of shShank3 virus (50 nL; Supplementary Fig. 6a-g), while no difference was found in a test of social memory between shShank3 mice and controls (Supplementary Fig. 6h-k), strengthening the case for specific involvement of VTA in social preference.

To examine whether impaired social preference was accompanied by a generalized anhedonic behavior, that is, a reduction in the interest for natural reward, we performed a sucrose preference test by comparing intake of different sucrose concentrations to water (Supplementary Fig. 6l-o). ShShank3 mice preferred a sucrose solution at high concentration, but not at the low concentration. However, it should be noted that shShank3 mice consumed significantly more water during the low sucrose concentration condition (Supplementary Fig. 6m), which led to the observed decreased sucrose preference ratio

(Supplementary Fig. 6l). Taken together, it is unclear how broadly VTA-SHANK3 insufficiency affects behaviors motivated by natural rewards.

Finally, mice were assessed for general activity levels in an open-field arena. There was no evidence for altered thigmotaxis or locomotor activity between shShank3 mice and controls (Supplementary Fig. 7a-c). However, during this test, shShank3 mice exhibited higher levels of self-grooming compared to scrShank3 controls (Supplementary Fig. 7d). Although levels of self-grooming were insufficient to induce skin lesions, these observations provide some, albeit limited, evidence for increased repetitive behavior following VTA-SHANK3 insufficiency. No differences in body weight were observed between scrShank3 and shShank3 vehicle treated mice (Supplementary Fig. 7e,f). Collectively, our behavioral analyses indicate that VTA-SHANK3 insufficiency leads to behavioral alterations including decreased time-dependent conspecific interactions and increased self-grooming.

Requirement for VTA DA neuron activity in social preference

Could impaired social preference be ascribed to altered function of VTA DA or GABA neurons? Since PAM-mGluR1 treatment acted to specifically normalize DA neuron synaptic function and activity (Fig 4 and 5), we took advantage of this finding to examine whether this cell-type specific rescue would be sufficient to normalize social behavior. Thus, following early postnatal intra-VTA AAV-shShank3 or scrShank3 injections, mice received once daily systemic injections of PAM-mGluR1 during the period of synapse maturation (P6-P27) until 24 h before the three-chamber social interaction test (Fig. 6a). While PAM-mGluR1 treatment did not affect social preference dynamics in scrShank3 control mice, social preference dynamics were rescued in shShank3 animals (Fig. 6b-f; Supplementary Fig. 5a-h). Locomotor parameters, such as the velocity and distance travelled during the test did not differ between the groups (Supplementary Fig. 5i,j). These data indicate that altered VTA Putative DA neuron function is a key mechanism by which VTA-SHANK3 insufficiency generates impaired social preference.

Is the rescue of postnatal maturation with mGluR1-PAM permanent? To test this possibility, we down-regulated SHANK3 during the early postnatal period, then treated the mice with the mGluR1-PAM (P6-P27) and looked at synaptic transmission and behaviors in adult animals (Fig. 7a). In control shShank3 mice that received vehicle instead of the mGluRl-PAM, we observed a high AMPA/NMDA ratio (Fig. 7b) and a reduction in social preference during T_2 (Fig. 7c), replicating findings described above. In contrast, PAM-mGluR1 treatment during early life reduced the AMPA/NMDA ratio (Fig. 7b) and normalized social preference (Fig. 7c,d). Thus, mGluR1 PAM treatment during postnatal development ameliorates both, synaptic alterations and behavioral deficits caused by SHANK3 insufficiency.

This pharmacological rescue suggests that normal VTA DA neuron activity may be sufficient for the maintenance of social preference. We performed optogenetic stimulation of VTA DA neurons during the three-chamber social interaction test in shShank3 injected mice. Channelrhodopsin (ChR2) was selectively expressed in VTA DA neurons by injecting AAV-DIO-ChR2 into the VTA of DAT-Cre mice previously infected with shShank3 or scrShank3 (Fig. 8a,b). To validate the approach, blue light stimulation induced reliable bursts of action

potentials in VTA DA neurons recorded from acute slices of shShank3 mice (Fig 8c,d). *In vivo,* we stimulated VTA DA neurons35 during T2 when mice were in close proximity to the social stimulus (Fig. 8e). ShShank3 mice that did not receive optogenetic stimulation showed a reduction in social preference at T2 (Fig. 8f,g). However, phasic stimulation of VTA DA neurons increased social preference during T2 in both scrShank3 and shShank3 mice (Fig. 8f) and increased normalized social preference of shShank3 mice to levels of scrShank3 control group (Fig. 8g). These findings demonstrate the sufficiency of DA neuron activity to support social preference and show that such stimulation protocols can overcome impaired social behavior owing to SHANK3 downregulation.

Discussion

With a growing body of evidence pointing to the involvement of VTA in both social behavior and repetitive actions3,4, our study examines whether and how deficits in these behavioral domains could arise from haploinsufficiency of a gene linked to ASD. We find that VTA-SHANK3 downregulation alters excitatory transmission onto both DA and GABA neurons. Together they dampened the firing activity of DA neurons, with an impact on social preference. Treatment with a mGluR1 PAM during the initial period of postnatal development is sufficient to reverse deficits in social preference, which remain normal in adult animals. Moreover, DA neuron burst firing activity is sufficient to support social preference and overcome social impairments arising from VTA-SHANK3 insufficiency. Taken together, our study argues for a central role of perturbed VTA DA neuron maturation in the development of social preference.

Several mouse models have been generated to study the consequences of *Shank3* deletion33. Focusing on the postsynaptic density of striatal neurons, a reduction in the expression of GluA2, GluN2A and GluN2B has been observed in *Shank3* KO mice lacking the PDZ-containing SHANK3 isoforms16. In mouse models targeting the Ankyrin-repeated domain of SHANK3, a reduction in the expression of GluA1 and GluN2A subunits have been reported in the hippocampus, although no changes in basal synaptic transmission were found18. Meanwhile, deletion of exon 21 reveled no major changes in synaptic ionotropic receptor subunits in whole hippocampal homogenates19. Here, we find that downregulation of the proline-rich domain-containing isoforms of SHANK3 has different consequences on basal synaptic transmission depending on the neuronal cell type within the same brain region. Specifically, the AMPAR subunit composition was altered only at excitatory synapses onto DA neurons, where SHANK3 downregulation promoted the insertion of GluA2-laking AMPARs. However, in VTA GABA neurons, SHANK3 downregulation changed the AMPA/NMDA ratio but left the AMPAR subunit composition unaffected. Taken together, the variety of synaptic alterations reported in different mutant mouse models may reflect disruptions of distinct *Shank3* domains, whose expression is further regulated in a brain region and cell-type specific manner.

In VTA DA neurons, activation of mGluR1 during postnatal development drives synaptic maturation by exchanging GluA2-lacking for GluA2-containing AMPARs21. This may establish competent DA neuron function, which in adulthood is required to assign emotional valence to salient stimuli36. We find that SHANK3 downregulation prevents the postnatal

maturation of AMPAR transmission onto VTA DA neurons and synapses remain in an immature state. Thus, SHANK3 may serve to guarantee optimal functionality of mGluR1 and its signaling pathway during synaptic maturation of VTA DA neurons. Boosting mGluR1 signaling with a PAM during the period of synaptic development may overcome SHANK3 deficiency and drive the exchange of immature for mature receptors onto VTA DA neurons. Surprisingly, at excitatory synapses onto VTA GABA neurons, we did not observe the presence of GluA2-lacking AMPARs when SHANK3 was downregulated and mGluR1 PAM treatment was unable to rescue synaptic deficits. These findings are in agreement with our previous observations that mGluR1-LTD is contingent of the presence of GluA2-lacking AMPARs at the synapses26. A different expression of group-I mGluRs37, a different synaptic localization of SHANK3 or mechanisms of synaptic maturation that may differ between VTA DA and GABA neurons could also explain our results.

Interfering with the expression of *Shank3* in the VTA triggers multiple alterations in synapses and circuits that together reduce DA neuron activity. Other studies have shown that SHANK3 insufficiency can alter cell morphology15, and DA and GABA morphological changes should be examined in future studies. At the cellular level, reduced DA neuron activity could arise from a change in mGluR1 signaling following SHANK3 downregulation. Indeed, burst activity of DA neurons is regulated by NMDA and Group I mGluRs activation29. Precisely how changes in excitatory synaptic transmission and cell-intrinsic properties interact to determine DA neuron activity warrants further investigation. In addition, VTA DA neurons receive inhibition from local GABA neurons32,38, whose increased activity following SHANK3 downregulation may further dampen the activity of the DA neurons. Nevertheless, the central role for DA neuron activity in supporting social interactions is supported by our findings that restoring synaptic transmission onto DA neurons with mGluR1 PAM treatment or optogenetic activation of DA neurons were both sufficient to rescue normal social behavior in VTA-SHANK3 deficient mice.

How might perturbed VTA DA neuron activity lead to deficits in social behavior? Several studies have implicated DA in social bonding39,40. It has been suggested that DA neuron activity directly influences social choice41 and facilitates choice of familiar partners42. Recently, it has been shown that activity of DA neurons, measured by monitoring cellular calcium dynamics, increases during social but not object interaction9. Since DA neurons project widely throughout the corticolimbic system, it would be interesting to understand how regions downstream of VTA DA neurons contribute to behavioral impairments reported here. Projections to the NAc may be particularly relevant, since their activity predicts social interactions in freely moving mice, possibly by controlling the firing of D1 Receptor expressing medium spiny neurons9.

In addition to impaired social behavior, VTA-SHANK3 downregulation also elevated self-grooming and altered sucrose preference, albeit only at low sucrose concentrations. These findings may reflect a more general deficit in processing natural rewards, which could contribute to the failure of shShank3 mice to maintain social preference. Alternatively, since reduced sucrose preference was seen in the context of increased water consumption, this observation together with elevated self-grooming may point to increased repetitive behaviors in VTA-SHANK3 mice. Although more robust and precise assays for repetitive behaviors

are needed to firmly establish this, repetitive behaviors have been observed in several other Shank3 mouse models16,18 and are thought to recapitulate the repetitive behavior observed in ASD patients. Dopamine has been linked to repetitive behaviors in several studies *via* its actions on corticostriatal circuits43. Since our manipulation is selective for the VTA, the repetitive behaviors observed may arise from altered function of ventral striatum, producing changes in the motivational aspects of behavioral control. A future challenge is to understand how the encoding of distinct repetitive and social behaviors is distributed across mesocorticolimbic circuits.

Finally, our study confirms mGluR1 activation in VTA DA neurons during the early postnatal period as an essential determinant of postnatal development, which may be deficient in certain forms of ASD. We provide a proof of principle that under conditions of low SHANK3 levels, treatment with a positive allosteric modulator of mGluR1 can overcome deficits in postnatal development. However, it's unknown whether the VTA dysfunction and response to mGluR1 modulation observed in VTA-SHANK3 mice is also present in global loss-of-function *Shank3* mutants that more closely reflect the etiology associated with *SHANK3* mutations found in ASD cases. Nevertheless, the pharmacological rescue of both neuron function and behavior in VTA-SHANK3 mice persists into adulthood and suggests that mGluR1 may be a valid target for the early treatment of some form of ASDs.

Matherial and Methods

Animals

The study was conducted with wild type C57B1/6j (WT), DAT-iresCre (*Slc6a3*$^{tm1.1(cre)Bkmn}$) and GAD-Cre (65 kDa isoform of the *Gad2* locus44) male and female mice housed in groups (weaning at P21-P23) under normal light-dark cycle (light on 7.00 am). All the physiology and behavior experiments were performed during the light cycle. All the procedures performed at the UNIL and UNIGE compiled with the Swiss National Institutional Guidelines on Animal experimentation and were approved by the Swiss Cantonal Veterinary Office Committee for Animal Experimentation. All procedures performed at Bordeaux were conducted in accordance with the European directive 2010-63-EU and with approval from Bordeaux University Animal Care and Use Committee (no. 50120205-A). All experiments were performed blindly to the experimenter and within each litter the mice were randomly assigned to both virus and pharmacological treatments.

The number of animals used for each experiment is reported per group in each figure legend. No statistical methods were used to pre-determine sample sizes but our sample sizes are similar to those generally employed in the field.

Electrophysiology

200-250 μm thick horizontal midbrain slices containing VTA were prepared following the experimental injection protocols described in the text. Slices were kept in artificial cerebrospinal fluid containing 119 mM NaCl, 2.5 mM KCl, 1.3 mM $MgCl_2$, 2.5 mM $CaCl_2$, 1.0 mM NaH_2PO_4, 26.2 mM $NaHCO_3$ and 11 mM glucose, bubbled with 95% O2 and 5%

CO_2. Whole-cell voltage-clamp recording techniques were used (30–32 °C, 2–3 ml min−1, submerged slices) to measure the holding currents and synaptic responses of VTA neurons, with recordings made medially to the Medial Terminal nucleus of the accessory optic tract (MT). Putative DA and GABA neurons were classified accordingly to the following criteria: large/small soma, cell capacitance (for putative DA neuron > 28 pF, for putative GABA neuron < 27 pF), hyperpolarization step (-60 mV, 500 msec duration immediately after whole-cell patch clamp configuration) induced I_h current presence/absence and input resistance (monitored for 2 minutes after the whole-cell patch clamp configuration at +40 mV). Recordings were performed from Non Infected, shShank3 and scrShank3 infected cells (identified by the expression of the green reporter protein) and sorted as putative DA or putative GABA neurons as described above. The internal solution contained 130 mM CsCl, 4 mM NaCl, 2 mM $MgCl_2$, 1.1 mM EGTA, 5 mM HEPES, 2 mM Na_2ATP, 5 mM sodium creatine phosphate, 0.6 mM Na_3GTP and 0.1 mM spermine. Currents were amplified, filtered at 5 kHz and digitized at 20 kHz. The liquid junction potential was small (−3 mV) and traces were therefore not corrected.

Access resistance was monitored by a hyperpolarizing step of -14 mV at each sweep, every 10 s. The cells were recorded at the access resistance from 10–30 MΩ for putative DA neurons and 15-40 MΩ for putative GABA neurons. Data were excluded when the resistance changed > 20%. Synaptic currents were evoked by stimuli (0.05–0.1 msec) at 0.1 Hz through a stimulating electrode placed rostral to the VTA. The experiments were carried out in the presence of $GABA_A$ receptor antagonist picrotoxin (100 μM); the AMPAR-EPSCs were pharmacologically isolated by application of the NMDAR antagonist D-APV (50μM) and NMDAR EPSCs were recorded at +40 mV in presence of the AMPAR blocker NBQX (10 μM). Representative example traces are shown as the average of 15-20 consecutive EPSCs typically obtained at each potential. The rectification index of AMPARs is the ratio of the chord conductance calculated at negative potential (-60 mV) divided by the chord conductance at positive potential (+40 mV). The analysis of the decay time of NMDAR-mediated EPSC was conducted as described previously45 and the Ifenprodil sensitivity was calculated as the percentage of NMDAR-EPSC amplitude reduction (at +40 mV) after 20-25 minutes of continuous Ifenprodil (3 μM, GluN2B-containing NMDAR antagonist) bath-application compared to baseline. The time interval between the two stimulations for the Paired Pulse Ratio (PPR) measurement was 50 msec (Inter Stimulation Interval, ISI) and the ratio was obtained by dividing the $EPSC_2$ by $EPSC_1$ amplitude at -60 mV. The *in vitro* validation of the optogenetic protocol (used *in vivo*) was performed in current-clamp configuration, after the assessment of the I_h current and the desensitization current (500 msec pulse duration) in voltage-clamp. The internal solution contained 140 mM K-Gluconate, 2 mM $MgCl_2$, 5 mM KCl, 0.2 mM EGTA, 10 mM HEPES, 4 mM Na_2ATP, 0.3 mM Na_3GTP and 10 mM Creatine-Phosphate. Blue-light was delivered through the 40X objective focused on the cell soma with a power intensity of 8 mW. The Synaptic responses were collected with a Multiclamp 700B-amplifier (Axon Instruments, Foster City, CA), filtered at 2.2 kHz, digitized at 5 Hz, and analyzed online using Igor Pro software (Wavemetrics, Lake Oswego, OR).

Stereotaxic injections

Injections of purified AAV-shShank3, AAV-scrShank3 and AAV-CAG-DIO-tdTomato were performed in mice at different time points. The anaesthesia was induced and maintained with a mixture of Oxygen and Isoflurane (Baxter AG, Vienna, Austria). The animals were then placed on the stereotaxic frame (Angle One; Leica, Germany) and a single or bilateral craniotomy was made over the VTA at following stereotaxic coordinates: for neonatal injections (P2-P5) ML 0.15 mm, AP 0.1 mm, DV -3.8 mm from Lambda; for juvenile injections (P14/P21/P24) ML ±0.5 mm, AP -3.2 mm, DV -4.0 mm from Bregma. The virus was injected with graduated pipettes (Drummond Scientific Company, Broomall, PA) at the rate of 100 nl/min for a total volume of 50 and 200 nL for neonatal (as reported in the text) and 400 nL for juvenile animals. For all the experiments the virus was incubated for at least 9 days, when expression was clearly identifiable by the reporter protein expression, before proceeding with further manipulations.

In vivo single-unit neuron recordings

A glass micropipette (tip diameter: 2-3 μm; 4-6 MΩ for VTA dopamine neurons and tip diameter: 1-2 μm, 10-15 MΩ for VTA putative GABA neurons) filled with 2% pontamine sky blue solution in 0.5 M sodium acetate was lowered into the VTA. VTA dopamine neurons were identified according to well-established electrophysiological features46–48, which included the following: (1) an action potential with ≥ 1.1 ms (measured from the start of action potential to the negative trough); (2) slow spontaneous firing rate (≤ 10 Hz); (3) single and burst spontaneous firing patterns composed by 2 to 10 spikes *in vivo* . The onset of a burst was defined with an interspike interval lower than 80 msec and the end of the burst with an interspike interval higher than 160 msec31. Putative VTA GABA neurons were identified according to well-established electrophysiological criteria (1) an action potential width <1.1 m; (2) VTA boundary was defined 200 μm dorsal to the first VTA DA neuron recorded31,32,49,50. The extracellular potential was recorded with an Axoclamp-2B amplifier and filter (300 Hz/0.5 kHz;51). Single neuron spikes were collected online (CED 1401, SPIKE 2; Cambridge Electronic Design). Four parameters for VTA dopamine neuron firing and bursting activity were analyzed: the cumulative probability distribution of the firing rate and the bar graphs with the mean ± SEM, the bursting rate, the index of bursting (burst event frequency × mean spikes per burst). Results are expressed as mean ± SEM.

Immunohistochemistry and cell counting

Mice were sacrificed and trans-cardially perfused with PBS 1X followed by 4% paraformaldehyde prepared in PBS 1X. The brain was removed and left for overnight post-fixation at 4°C. Horizontal VTA slices were cut at 50 μm and washed three times in PBS 1X before incubation in the blocking solution containing 0.3% Triton X-100 and 1% goat serum. The slices were incubated with rabbit anti-TH (Abcam ab112, 1:500) at 4°C overnight and then washed three times in PBS 1X and incubated for 2 hours at room temperature with secondary antibodies, goat anti-rabbit IgG-Alexa 568 (abcam, 1:500; ab175471) or goat anti-rabbit IgG-Alexa 647 (abcam, 1:500; ab150079). Finally, the slices were washed three times in PBS 1X before being mounted onto microscope slides with

Abcam DAPI-mounting medium (abcam, ab104139). Images were acquired with an LSM-710 confocal microscope.

Cell counting was performed on 50 μm thick VTA slices from at least 4 WT mice and 3 GAD-Cre mice injected with shShank3 (at P5) and AAV-CAG-DIO-tdTomato (at P14). All slices were collected and immunohistochemistry against TH was performed for every other slice (secondary antibody IgG-Alexa 568 for WT and IgG-Alexa 647 for GAD-Cre:tdTomato mice). Two confocal images of VTA were acquired bilaterally for each slice, along the whole VTA dorso-ventral axis in the dopaminergic area. For WT, the number of TH^+, $ZsGreen^+$, TH^+-$ZsGreen^+$ cells were counted in at least 6 fields of view per mouse, and a percentage average calculated for each mouse. The total percentage average (Supplementary Fig. 1b) was calculated as an average of the values from each mouse. For the cell-counting of the total number of TH-positive cells, the VTA was unilaterally infected and sliced at juvenile stage and cell counting performed as described above (Supplementary Fig. 1c). Cell-counting from GAD-Cre:tdTomato was performed by two independent experimenters. Specifically, the number of TH^+, TH^+-$ZsGreen^+$, $tdTom^+$, $tdTom^+$-$ZsGreen^+$ was counted in each field of view of the VTA along the whole dorso-ventral axis (at least 6 fields). The percentage of cells obtained by each experimenter was averaged for each mouse. The total percentage of infected cells (Fig. 1b) was obtained by averaging the percentage obtained for each mouse.

Western blot analysis

AAV-shShank3 and AAV-scrShank3 infected mice (P21-P35) were anaesthetized and decapitated. 350 μm thick midbrain slices were obtained with a vibratome (Leica VT1200S). The VTA and the adjacent SN were dissected in animals that showed virus expression (1 mouse was excluded from shShank3 group because not infected), isolated and homogenized in a lysis buffer containing 20 mmol/L HEPES, pH 7.4, 10 mmol/L NaCl, 3 mmol/L MgCl2, 2.5 mmol/L EGTA, 0.1 mmol/L dithiothreitol, 50 mmol/L NaF, 1 mmol/L Na3VO4, 1% Triton X-100, and a protease inhibitor cocktail (Roche). Lysates were boiled for 5 min and separated on a denatureting 5-9% acrilamide gel. The following primary antibodies were used: Shank 3 (H-160) (sc-30193, Santa Cruz Biotechnology, 1:200) and -Tubulin (sc-8035,Santa Cruz Biotechnology, 1:1000). The following secondary antibodies were used: goat-anti-rabbit, goat-anti-mouse coupled with IRdye 800 or IRdye 680 (936-32210, 926-32220, LiCor, Lincoln, 1:10.000) in 30%. Protein bands were revealed by the Odyssey infrared image system (LiCor).

Social Interaction Test

A three-chambered social preference test was used, comprising of a rectangular Plexiglas arena (60×40×22cm) (Ugo Basile, Varese, Italy) divided into three chambers (each 20 × 40 × 22 (h) cm). The walls of the center chamber had doors that could be lifted to allow free access to all chambers. The social preference test was performed similarly as published by Moy et al.52 and the variables were scored and calculated as previously published53.

Briefly, each mouse was placed in the arena for a habituation period of 10 minutes, when it was allowed to freely explore the empty arena. At the end of the habituation, the test was

performed when two enclosures with metal vertical bars were placed diagonally, one in the bottom left corner of the left and one in the top right corner of the right compartment. One enclosure was empty (serving as an inanimate object) whereas the other contained a social stimulus (unfamiliar juvenile mouse 25 ± 1 days old). The enclosures allowed for visual, auditory, olfactory and tactile contact between the experimental mice and the mice acting as social stimuli. The juvenile mice in the enclosures where habituated to the apparatus and the enclosures for a brief period of time on the 3 days preceding the experiment. The experimental mouse was allowed to freely explore the apparatus and the enclosures for 10 minutes. The position of the empty vs. juvenile-containing enclosures alternated and was counterbalanced for each trial to avoid any bias effects.

Every session was video-tracked and recorded using Ethovision XT (Noldus, Wageningen, the Netherlands), which provided an automated recording of the entries around the enclosures, the distance moved and the velocity. Behavior was also manually scored by an experimenter blind to the treatment of animals. The mice were considered to explore the empty and the social stimulus when their nose was directed towards the enclosures' contents at a distance less than approximately 2 cm. The time spent sniffing each enclosure was assessed and then used to determine the preference score for the social target as compared to the empty enclosure (social/ (social + empty)). To investigate the dynamics of social preference between groups across time, we divided the test phase in two 5-minute bins and calculated the social preference ratios for these two time-points (T_1 and T_2). Moreover, the normalized social preference at T_2 (SP_2) was calculated by dividing the social preference score at T_2 by the social preference score for the total testing time. The change in the interaction with the mouse was calculated between T_1 and T_2 (time of interaction with social target at T_2 - time of interaction with social target at T_1) and similarly the change in interaction for the empty enclosure was calculated. The arena was cleaned with 1% acetic acid solution and dried properly between trials.

Social Memory Task

For the cohort of mice injected in the VTA with 50nL of AAV-shShank3 or AAV-scrShank3 a social memory task was performed. Following the social preference test performed as described above, a novel mouse was introduced into the formerly empty enclosure. Mice were exposed to the enclosures containing the novel and the familiar mouse for 10 minutes. Time spent sniffing each enclosure was assessed and the preference score for the novel mouse compared to the familiar (novel/ (novel + familiar)) was calculated. The social memory test was also divided in two 5-minute bins and social memory calculated during time-point 1 (T_1) and 2 (T_2). As reported for the social preference test, the normalized social memory at T_2 (SM_2) was calculated by dividing the social memory score at T_2 by the social memory score for the total testing time. The change in the interaction with the novel mouse was calculated between T_1 and T_2 (time of interaction with novel mouse at T_2 - time of interaction with novel mouse at T_1) and similarly the change in interaction was calculated for the familiar mouse.

Optogenetic Stimulation during the social preference test

AAV-shShank3 and AAV-scrShank3 infected DATCre mice underwent a second stereotaxic surgery at 4-5 weeks of age to inject 250-500nL of AAV5-ef1a-ChR2(H134R)-eYFP into the VTA (-3.2 AP, +0.9 ML and -4.28 DV at a 10° angle), together with a single fiber optic cannula at the same coordinates, but positioned approximately 0.1 mm above the ChR2 infection site35 . Following at least two weeks of recovery, mice were first habituated to a patch cable during 3 × 30 minute sessions preceding the social preference test. The social preference test was performed as described above, except that mice assigned to the 'ON' condition received phasic blue light stimulation of VTA DA neurons when they entered in close proximity to the social stimulus only during T_2. Laser power was controlled between each test to ensure an estimated 7-10 mW of power at the implanted fiber tip.

Open Field Test

The open field was a 75 cm diameter, Plexiglas circular arena, divided into three virtual zones (wall, intermediate and center). Animals were allowed to freely explore the open field for 10 minutes and their behavior was automatically (Ethovision, Noldus, Wageningen, the Netherlands) and manually scored (for assessing self-grooming behavior). Parameters analyzed with the automated tracking system were distance, velocity and time in the different zones. The arena was cleaned with 1% acetic acid and dried between each test.

Sucrose Preference Test

Mice were housed individually for the duration of this task (48 hours) and had access to standard lab chow and tap water throughout the experiment. At 18h00 they were exposed to two drinking bottles, one with water and the other one containing sucrose solution. During the first testing day, sucrose was given at 1% and 24 hours afterwards the bottles were weighed and subsequently the sucrose solution was given to the mice at a concentration of 8% for another 24 hours, when the second measurement was taken. Mice were weighed at the beginning of the experiment and water and sucrose bottle positions were counterbalanced between animals to avoid any confounding effect of side preference. Sucrose and water consumption were normalized to 10 grams of the body weight of each mouse and the amount of water and sucrose drunk was analyzed. A sucrose preference ratio was calculated as (sucrose consumed/ (sucrose consumed + water consumed)).

Drugs and viruses

AAV-shShank3/scrShank3 (AAV5, AAV1; 7.4×10^{13} GC/mL; VectorBioLab); AAV-CAG-DIO-tdTomato (AAV9, gift from Prof. Anthony Holtmaat), rAAV5-Ef1a-DIO-hChR2(H134R)-eYFP (5×10^{12} virus molecules/mL UNC), Ro 677476 (4346, Tocris), D-APV (0106, Tocris), Picrotoxin (1128, Tocris), NBQX (0373, Tocris), (R,S)-3,5-DHPG (0342, Tocris), Ifenprodil hemitartrate (0545, Tocris).

Statistical Analysis

The data were analyzed with independent or paired two-tailed samples t-tests, one-way, two-way or repeated measures analysis of variance (ANOVA) followed up by post hoc tests (reported in the figure legend). Normality was checked with the Shapiro-Wilk criterion and

when violated, non-parametric statistics were applied (Mann-Whitney and Kruskal-Wallis). Regarding t-tests, when Levene's test for the equality of variances was significant, suggesting that equal variances are not assumed, the adjusted values and degrees of freedom are reported. All bars and error bars represent the mean ± the standard error of the mean (SEM) respectively and the significance was set at $p < 0.05$. The data were analyzed using the statistical package SPSS (SPSS, Chicago, IL, USA) versions 17.0 and 22.0 and Graphpad Prism 5 and 6 and the graphs were created using GraphPad Prism 5 and 6 (San Diego, CA, USA). For the behavioral experiments two animals out of sixty were excluded from the analysis, as one was not infected in the VTA (shShank3:Vehicle) and another did not show any social preference during T_1 (scrShank3:Ro). A supplementary methods checklist is available.

Data availability

The data that support the findings of this study are available from the corresponding author upon request.

Supplementary Material

Refer to Web version on PubMed Central for supplementary material.

Acknowledgements

C.B is supported by the Swiss National Science Foundation, Pierre Mercier Foundation and NCCR Synapsy. C.L. is supported by the Swiss National Science Foundation and by the European Research Council (MeSSI Advanced grant). This work was supported by a grant from the Simons Foundation (SFARI #239496 to C.L.). We thank Manuel Mameli, Denis Jabaudon and Fabrizio Gardoni for the critical reading of the manuscript.

References

1. Volkmar FR, State M, Klin A. Autism and autism spectrum disorders: diagnostic issues for the coming decade. Journal of Child Psychology and Psychiatry. 2009; 50:108–115. [PubMed: 19220594]
2. Landa RJ. Diagnosis of autism spectrum disorders in the first 3 years of life. Nat Clin Pract Neurol. 2008; 4:138–147. [PubMed: 18253102]
3. Ameis SH, Catani M. Altered white matter connectivity as a neural substrate for social impairment in Autism Spectrum Disorder. Cortex. 2015; 62:158–181. [PubMed: 25433958]
4. Wood J, Ahmari SE. A Framework for Understanding the Emerging Role of Corticolimbic-Ventral Striatal Networks in OCD-Associated Repetitive Behaviors. Front Syst Neurosci. 2015; 9:171. [PubMed: 26733823]
5. Zeeland AAS-V, Dapretto M, Ghahremani DG, Poldrack RA, Bookheimer SY. Reward Processing in Autism. Autism research : official journal of the International Society for Autism Research. 2010; 3:53–n/a. [PubMed: 20437601]
6. Chevallier C, Kohls G, Troiani V, Brodkin ES, Schultz RT. The social motivation theory of autism. Trends in Cognitive Sciences. 2012; 16:231–239. [PubMed: 22425667]
7. Schultz W. Predictive reward signal of dopamine neurons. J Neurophysiol. 1998; 80:1–27. [PubMed: 9658025]
8. Rodriguez Parkitna J, Engblom D. Addictive drugs and plasticity of glutamatergic synapses on dopaminergic neurons: what have we learned from genetic mouse models? Front Mol Neurosci. 2012; 5:89. [PubMed: 22969704]
9. Gunaydin LA, et al. Natural neural projection dynamics underlying social behavior. Cell. 2014; 157:1535–1551. [PubMed: 24949967]

10. Folstein SE, Rosen-Sheidley B. Genetics of autism: complex aetiology for a heterogeneous disorder. Nature Reviews Genetics. 2001; 2:943–955.
11. Zoghbi HY, Bear MF. Synaptic dysfunction in neurodevelopmental disorders associated with autism and intellectual disabilities. Cold Spring Harb Perspect Biol. 2012; 4:a009886. [PubMed: 22258914]
12. Phelan K, McDermid HE. The 22q13.3 Deletion Syndrome (Phelan-McDermid Syndrome). Mol Syndromol. 2012; 2:186–201. [PubMed: 22670140]
13. Gauthier J, et al. Novel de novo SHANK3 mutation in autistic patients. Am J Med Genet B Neuropsychiatr Genet. 2009; 150B:421–424. [PubMed: 18615476]
14. Boccuto L, et al. Prevalence of SHANK3 variants in patients with different subtypes of autism spectrum disorders. Eur J Hum Genet. 2013; 21:310–316. [PubMed: 22892527]
15. Naisbitt S, et al. Shank, a novel family of postsynaptic density proteins that binds to the NMDA receptor/PSD-95/GKAP complex and cortactin. Neuron. 1999; 23:569–582. [PubMed: 10433268]
16. Peça J, et al. Shank3 mutant mice display autistic-like behaviours and striatal dysfunction. Nature. 2011; 472:437–442. [PubMed: 21423165]
17. Bozdagi O, et al. Haploinsufficiency of the autism-associated Shank3 gene leads to deficits in synaptic function, social interaction, and social communication. Molecular Autism. 2010; 1:15. [PubMed: 21167025]
18. Wang X, et al. Synaptic dysfunction and abnormal behaviors in mice lacking major isoforms of Shank3. Hum Mol Genet. 2011; 20:3093–3108. [PubMed: 21558424]
19. Kouser M, et al. Loss of predominant Shank3 isoforms results in hippocampus-dependent impairments in behavior and synaptic transmission. J Neurosci. 2013; 33:18448–18468. [PubMed: 24259569]
20. Zhou Y, et al. Mice with Shank3 Mutations Associated with ASD and Schizophrenia Display Both Shared and Distinct Defects. Neuron. 2016; 89:147–162. [PubMed: 26687841]
21. Bellone C, Mameli M, Lüscher C. In utero exposure to cocaine delays postnatal synaptic maturation of glutamatergic transmission in the VTA. Nat Neurosci. 2011; 14:1439–1446. [PubMed: 21964489]
22. Bellone C, Lüscher C. Drug-evoked plasticity: do addictive drugs reopen a critical period of postnatal synaptic development? Front Mol Neurosci. 2012; 5:75. [PubMed: 22715323]
23. Verpelli C, et al. Importance of Shank3 protein in regulating metabotropic glutamate receptor 5 (mGluR5) expression and signaling at synapses. J Biol Chem. 2011; 286:34839–34850. [PubMed: 21795692]
24. Mameli M, Balland B, Luján R, Lüscher C. Rapid synthesis and synaptic insertion of GluR2 for mGluR-LTD in the ventral tegmental area. Science. 2007; 317:530–533. [PubMed: 17656725]
25. Argilli E, Sibley DR, Malenka RC, England PM, Bonci A. Mechanism and time course of cocaine-induced long-term potentiation in the ventral tegmental area. J Neurosci. 2008; 28:9092–9100. [PubMed: 18784289]
26. Bellone C, Lüscher C. Cocaine triggered AMPA receptor redistribution is reversed in vivo by mGluR-dependent long-term depression. Nat Neurosci. 2006; 9:636–641. [PubMed: 16582902]
27. Bellone C, Lüscher C. mGluRs induce a long-term depression in the ventral tegmental area that involves a switch of the subunit composition of AMPA receptors. Eur J Neurosci. 2005; 21:1280–1288. [PubMed: 15813937]
28. Knoflach F, et al. Positive allosteric modulators of metabotropic glutamate 1 receptor: characterization, mechanism of action, and binding site. Proc Natl Acad Sci USA. 2001; 98:13402–13407. [PubMed: 11606768]
29. Prisco S, Natoli S, Bernardi G, Mercuri NB. Group I metabotropic glutamate receptors activate burst firing in rat midbrain dopaminergic neurons. Neuropharmacology. 2002; 42:289–296. [PubMed: 11897107]
30. Meltzer LT, Serpa KA, Christoffersen CL. Metabotropic glutamate receptor-mediated inhibition and excitation of substantia nigra dopamine neurons. Synapse. 1997; 26:184–193. [PubMed: 9131777]
31. Ungless MA, Grace AA. Are you or aren't you? Challenges associated with physiologically identifying dopamine neurons. Trends Neurosci. 2012; 35:422–430. [PubMed: 22459161]

32. Tan KR, et al. GABA neurons of the VTA drive conditioned place aversion. Neuron. 2012; 73:1173–1183. [PubMed: 22445344]
33. O'Connor EC, Bariselli S, Bellone C. Synaptic basis of social dysfunction: a focus on postsynaptic proteins linking group-I mGluRs with AMPARs and NMDARs. Eur J Neurosci. 2014; 39:1114–1129. [PubMed: 24712991]
34. Crawley JN. Mouse behavioral assays relevant to the symptoms of autism. Brain Pathol. 2007; 17:448–459. [PubMed: 17919130]
35. Pascoli V, Terrier J, Hiver A, Lüscher C. Sufficiency of Mesolimbic Dopamine Neuron Stimulation for the Progression to Addiction. Neuron. 2015; 88:1054–1066. [PubMed: 26586182]
36. Stuber GD, et al. Reward-predictive cues enhance excitatory synaptic strength onto midbrain dopamine neurons. Science. 2008; 321:1690–1692. [PubMed: 18802002]
37. Merrill CB, Friend LN, Newton ST, Hopkins ZH, Edwards JG. Ventral tegmental area dopamine and GABA neurons: Physiological properties and expression of mRNA for endocannabinoid biosynthetic elements. Sci Rep. 2015; 5:16176. [PubMed: 26553597]
38. van Zessen R, Phillips JL, Budygin EA, Stuber GD. Activation of VTA GABA neurons disrupts reward consumption. Neuron. 2012; 73:1184–1194. [PubMed: 22445345]
39. Curtis JT, Wang Z. Ventral tegmental area involvement in pair bonding in male prairie voles. Physiology & Behavior. 2005; 86:338–346. [PubMed: 16165168]
40. Liu Y, Young KA, Curtis JT, Aragona BJ, Wang Z. Social bonding decreases the rewarding properties of amphetamine through a dopamine D1 receptor-mediated mechanism. J Neurosci. 2011; 31:7960–7966. [PubMed: 21632917]
41. Aragona BJ, Liu Y, Curtis JT, Stephan FK, Wang Z. A critical role for nucleus accumbens dopamine in partner-preference formation in male prairie voles. J Neurosci. 2003; 23:3483–3490. [PubMed: 12716957]
42. Aragona BJ, Wang Z. Dopamine regulation of social choice in a monogamous rodent species. Front Behav Neurosci. 2009; 3:15. [PubMed: 19707518]
43. Langen M, Kas MJH, Staal WG, van Engeland H, Durston S. The neurobiology of repetitive behavior: of mice…. Neuroscience & Biobehavioral Reviews. 2011; 35:345–355. [PubMed: 20156480]
44. Kätzel D, Zemelman BV, Buetfering C, Wölfel M, Miesenböck G. The columnar and laminar organization of inhibitory connections to neocortical excitatory cells. Nat Neurosci. 2011; 14:100–107. [PubMed: 21076426]
45. Bellone C, Nicoll RA. Rapid bidirectional switching of synaptic NMDA receptors. Neuron. 2007; 55:779–785. [PubMed: 17785184]
46. Ungless MA, Magill PJ, Bolam JP. Uniform inhibition of dopamine neurons in the ventral tegmental area by aversive stimuli. Science. 2004; 303:2040–2042. [PubMed: 15044807]
47. Grace AA, Bunney BS. Intracellular and extracellular electrophysiology of nigral dopaminergic neurons--1. Identification and characterization. Neuroscience. 1983; 10:301–315. [PubMed: 6633863]
48. McCutcheon JE, et al. Dopamine neurons in the ventral tegmental area fire faster in adolescent rats than in adults. J Neurophysiol. 2012; 108:1620–1630. [PubMed: 22723669]
49. Steffensen SC, Svingos AL, Pickel VM, Henriksen SJ. Electrophysiological characterization of GABAergic neurons in the ventral tegmental area. Journal of Neuroscience. 1998; 18:8003–8015. [PubMed: 9742167]
50. Bocklisch C, et al. Cocaine disinhibits dopamine neurons by potentiation of GABA transmission in the ventral tegmental area. Science. 2013; 341:1521–1525. [PubMed: 24072923]
51. Georges F, Aston-Jones G. Activation of ventral tegmental area cells by the bed nucleus of the stria terminalis: a novel excitatory amino acid input to midbrain dopamine neurons. J Neurosci. 2002; 22:5173–5187. [PubMed: 12077212]
52. Moy SS, et al. Sociability and preference for social novelty in five inbred strains: an approach to assess autistic-like behavior in mice. Genes Brain Behav. 2004; 3:287–302. [PubMed: 15344922]
53. Tzanoulinou S, Riccio O, de Boer MW, Sandi C. Peripubertal stress-induced behavioral changes are associated with altered expression of genes involved in excitation and inhibition in the amygdala. Transl Psychiatry. 2014; 4:e410. [PubMed: 25004390]

Europe PMC Funders Author Manuscripts

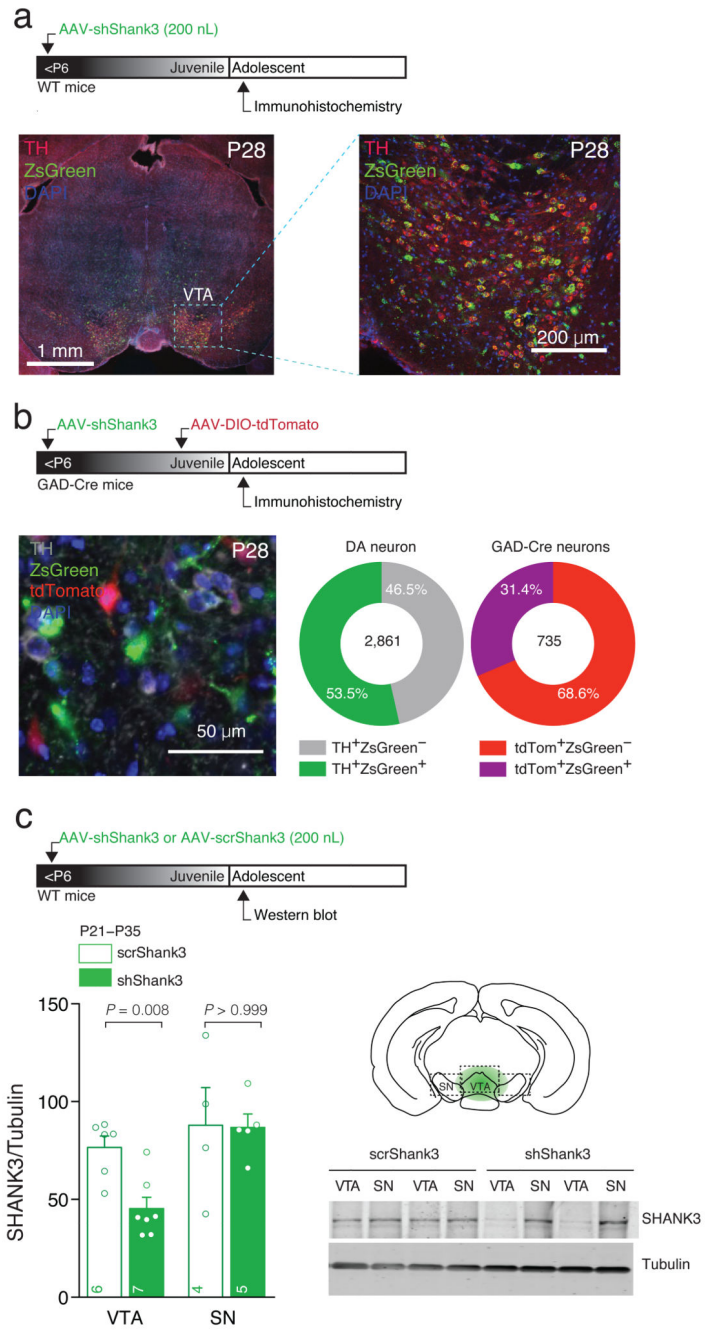

Fig. 1. Neonatal AAV-shShank3 infections target VTA DA and GABA neurons.

(**a**) Top: experiment schematic. Left: representative confocal image of coronal slice obtained from shShank3 infected WT mouse containing the VTA. Right: high magnification of VTA slice (**b**) Top: experiment schematic. Left: representative image of staining in GAD-Cre mice infected with shShank3 and DIO-tdTomato, identifying GABA neurons. Right: quantification of viral infection for DA and infected GAD-Cre VTA neurons (for details see Materials and Methods). (**c**) Top: Experiment schematic. Western blot quantification of SHANK3 downregulation in VTA and SN for scrShank3 and shShank3 injected WT mice

(VTA: Mann-Whitney $U = 3$; SN: Mann-Whitney U = 10). The numbers indicate the number of animals. Right: example of SHANK3 expression in scrShank3 or shShank3 VTA and SN.

Europe PMC Funders Author Manuscripts

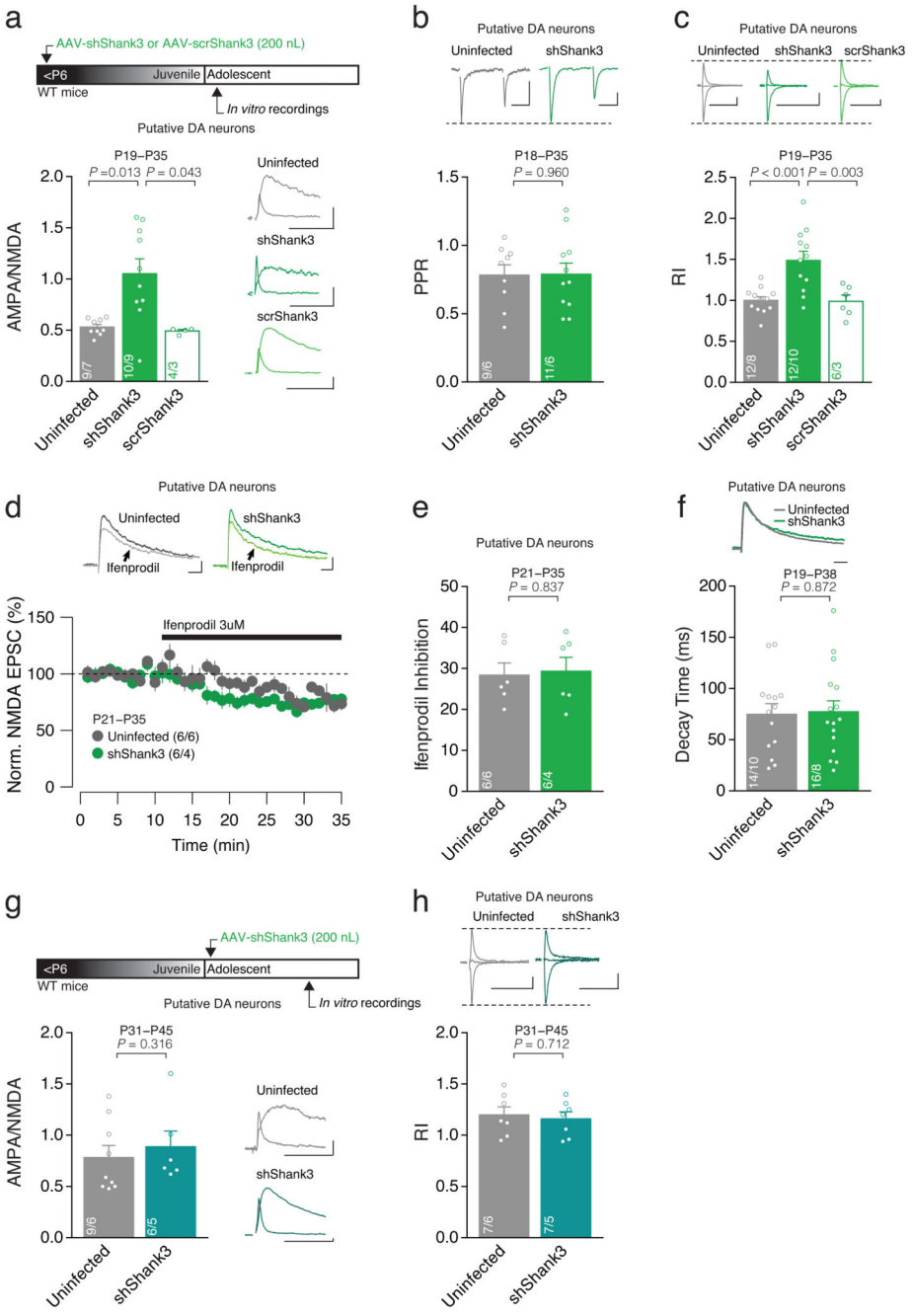

Fig. 2. Shank3 downregulation alters the postnatal development of AMPAR-mediated transmission.

(**a**) Top: experiment schematic. Group mean AMPA/NMDA ratio calculated in Uninfected, shShank3 and scrShank3 infected Putative DA neurons (Kruskal-Wallis $K_2 = 10.47$, $p = 0.005$, followed by Dunn's post hoc test). Right: example traces of evoked AMPAR- and NMDAR-EPSCs recorded at +40 mV. (**b**) Top: example traces of AMPAR-EPSC at -60 mV. Group mean PPR for shShank3 infected and Uninfected cells ($t_{18} = 0.05$, unpaired t-test). (**c**) Top: example traces of evoked AMPAR-EPSCs recorded at -60, 0 and +40 mV. Group mean

Europe PMC Funders Author Manuscripts

RI calculated in Uninfected, shShank3 and scrShank3 infected Putative DA neurons (one-way ANOVA $F_{2,27} = 11.66$, $p < 0.001$, followed by Tukey HSD post-hoc test). (**d**) Top: example traces of NMDAR-EPSCs during Ifenprodil (3 μM) bath application. Time course of NMDAR-EPSC amplitude during Ifenprodil application for Uninfected and shShank3 infected Putative DA neurons. (**e**) Group mean Ifenprodil inhibition calculated in Uninfected and shShank3 infected Putative DA neurons ($t_{10} = -0.21$, unpaired t-test). (**f**) Top: example traces of NMDAR-EPSC at +40 mV. Group mean decay time of NMDAR-EPSCs ($t_{28} = -0.16$, unpaired t-test). (**g**) Top: experiment schematic. Group mean AMPA/NMDA ratio calculated in Uninfected and shShank3 infected neurons ($U = 18.50$, Mann-Whitney test). Right: example traces of evoked AMPAR- and NMDAR- EPSCs recorded at +40 mV. (**h**) Group mean RI calculated in Uninfected and shShank3 infected Putative DA neurons ($t_{12} = 0.38$, unpaired t-test). Top: example traces of evoked AMPAR-EPSCs recorded at -60, 0 and +40 mV. Error bars show SEM. Example trace scale bar: 20 msec, 20 pA. The numbers indicate cells and mice.

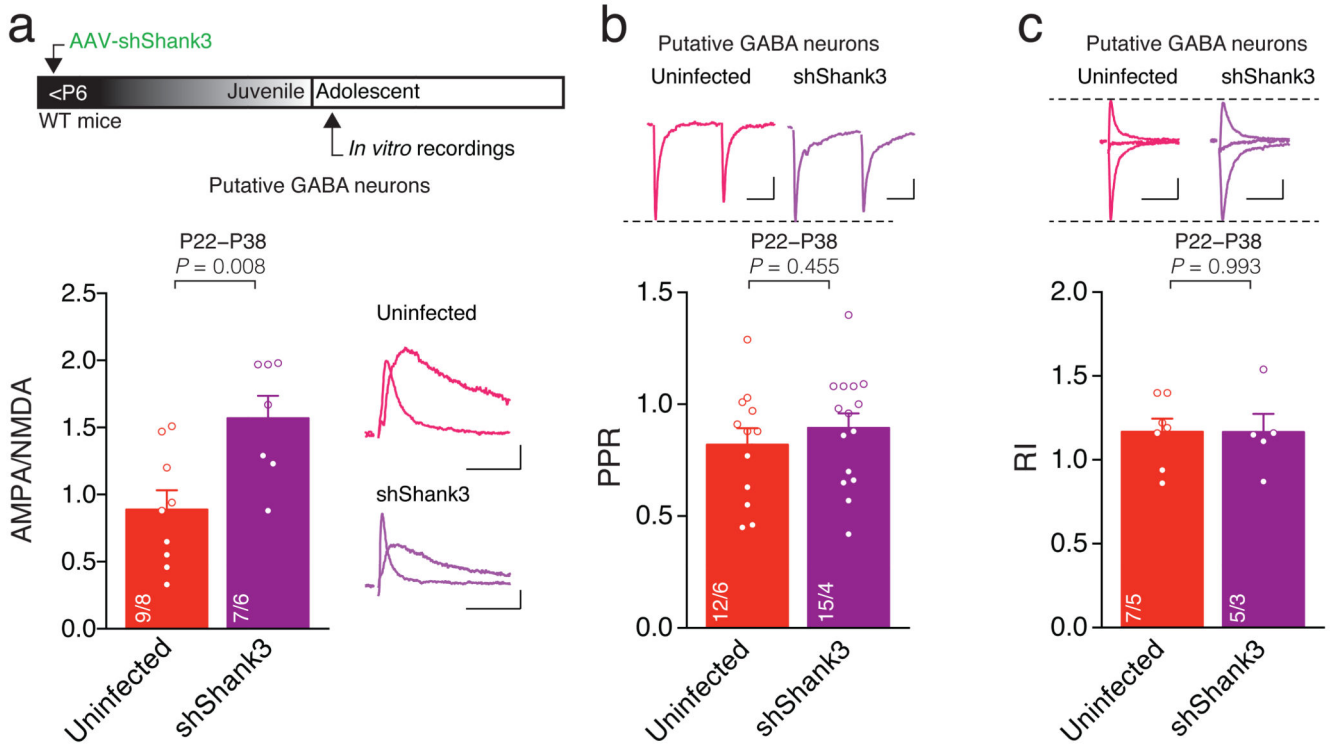

Fig. 3. Shank3 downregulation affects excitatory transmission onto VTA GABA neurons

(**a**) Top: experiment schematic. Group mean AMPA/NMDA ratio calculated in Uninfected and shShank3 infected Putative GABA neurons (t_{14} = -3.11, unpaired t-test). Right: example traces of evoked AMPAR- and NMDAR-EPSCs recorded at +40 mV. (**b**) Group mean PPR for Uninfected and shShank3 infected Putative GABA neurons (t_{25} = -0.76, unpaired t-test). Top: example traces of AMPAR-EPSC at -60 mV for Uninfected and shShank3 infected Putative GABA neurons. (**c**) Group mean RI calculated in Uninfected and shShank3 infected Putative GABA neurons (t_{10} = 0.01, unpaired t-test). Top: example traces of evoked AMPAR-EPSCs recorded at -60, 0 and +40 mV. Example trace scale bar: 20 msec, 20 pA. The numbers indicate cells and mice.

Europe PMC Funders Author Manuscripts

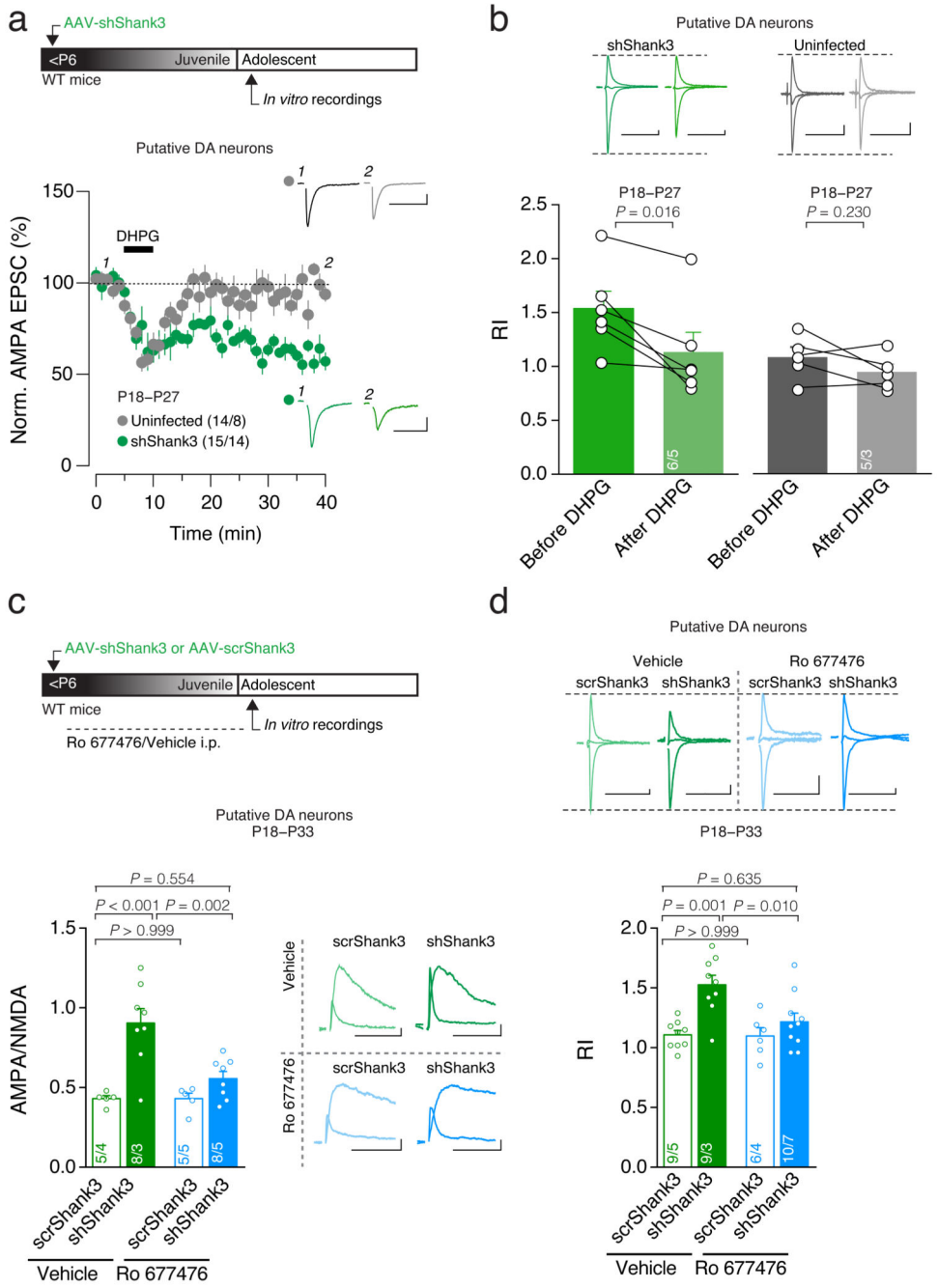

Fig. 4. Stimulation of mGluR1 rescues synaptic deficits

(**a**) Top: experiment schematic. Time course of pharmacologically isolated AMPAR-EPSCs recorded at -60 mV from Uninfected and shShank3 infected Putative DA neurons before and after 5 min application of DHPG (20uM). Inset: example traces of evoked AMPAR-EPSCs recorded at -60 mV. (**b**) Top: example traces of evoked AMPAR-EPSCs recorded at -60, 0 and +40 mV before and after DHPG application. Group mean RI before and 25 minutes after DHPG application (shShank3: $t_5 = 3.60$; Uninfected: $t_4 = 1.42$, paired t-test). (**c**) Top: experiment schematic. Group mean AMPA/NMDA ratio (two-way ANOVA; virus × drug

interaction: $F_{1,22} = 6.41$, $p = 0.019$; main effect virus: $F_{1,22} = 20.54$, $p < 0.001$; main effect drug: $F_{1,22} = 7.02$, $p = 0.015$; followed by Tukey HSD post-hoc test). Right: example traces of evoked AMPAR- and NMDAR-EPSCs recorded at +40 mV. (**d**) Top: example traces of evoked AMPAR-EPSCs recorded at -60, 0, +40 mV. Group mean RI (two-way ANOVA; virus × drug interaction: $F_{1,30} = 4.62$, $p = 0.040$; main effect virus: $F_{1,30} = 14.93$, $p = 0.001$; main effect drug: $F_{1,30} = 5.26$, $p = 0.029$; followed by Tukey HSD post-hoc test). Error bars show SEM. Example trace scale bar: 20 msec, 20 pA. The numbers indicate cells and mice.

Europe PMC Funders Author Manuscripts

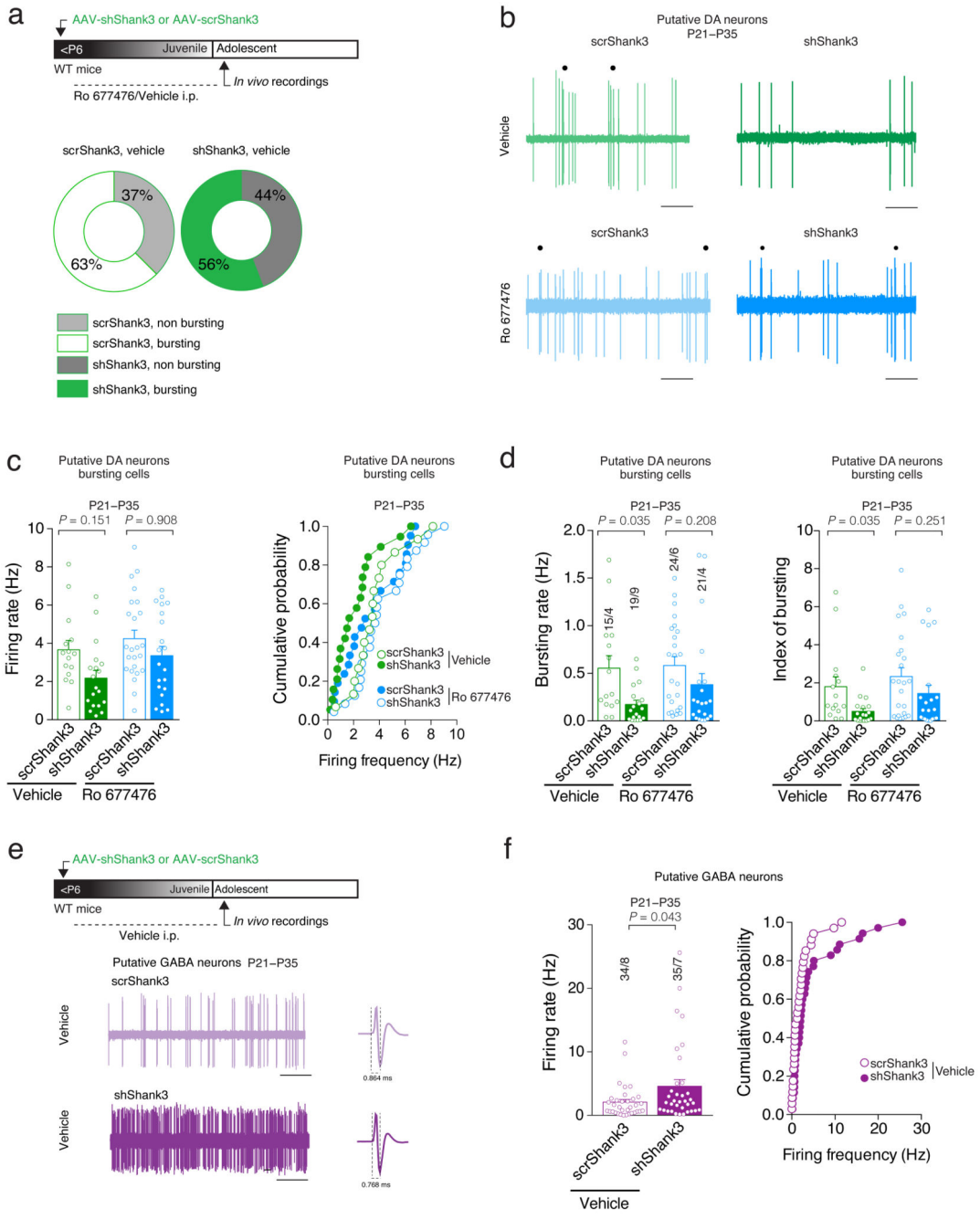

Fig. 5. VTA-Shank3 insufficiency alters *in vivo* DA neuron activity

(a) Top: experiment schematic. Quantification of bursting and non bursting VTA Putative DA neurons from scrShank3 or shShank3 vehicle treated mice. **(b)** Representative traces of a VTA Putative DA neuron recorded *in vivo*. Each dot represents a burst event. Scale bar: 1 s. **(c)** Group mean ± SEM and cumulative probability distribution of the firing rate of VTA Putative DA bursting cells (Kruskal-Wallis $K_3 = 10.85$, $p = 0.013$, followed by Dunn's post hoc test). **(d)** Effect of mGluR1-PAM (Ro 677476) treatment on bursting activity of VTA Putative DA neuron (for bursting rate: Kruskal-Wallis $K_3 = 14.09$, $p = 0.003$, followed by

Europe PMC Funders Author Manuscripts

Dunn's post hoc test; for index of bursting: Kruskal-Wallis $K_3 = 14.62$, $p = 0.002$, followed by Dunn's post hoc test). **(e)** Top: experiment schematic. Representative traces of VTA Putative GABA neurons recorded *in vivo.* Scale bar: 10s. **(f)** Group mean ± SEM (U= 425.5, Mann-Whitney test) and cumulative probability distribution of the firing rate of VTA Putative GABA neurons. The numbers indicate cells and mice.

Europe PMC Funders Author Manuscripts

Europe PMC Funders Author Manuscripts

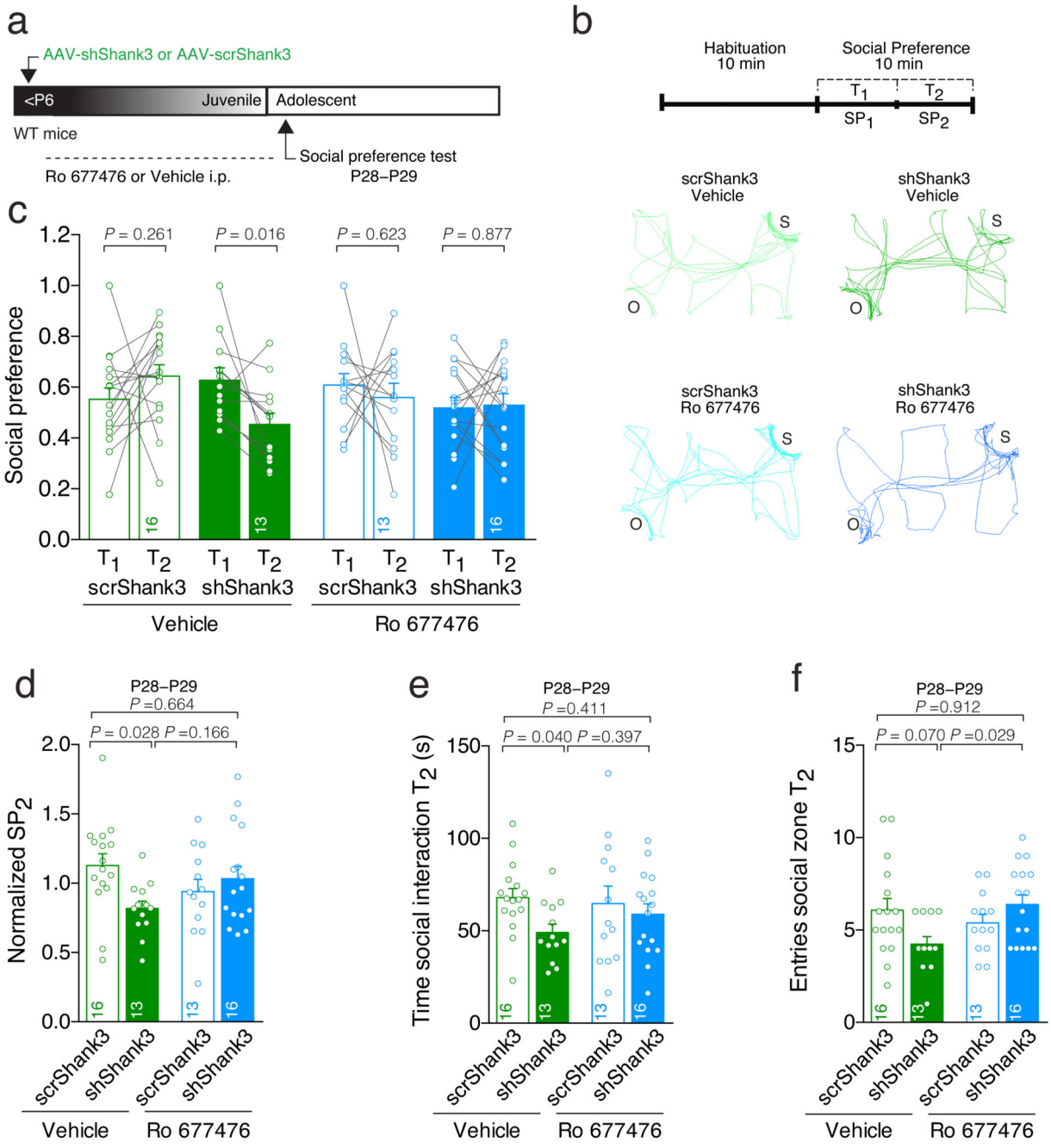

Fig. 6. VTA-SHANK3 insufficiency induces social deficits that are reversed by PAM-mGluR1 treatment.

(a) Experiment schematic. **(b)** Activity trail plots and experiment schematic (S: social target; O: inanimate object). **(c)** Scatter plots and group mean of social preference during the first half (T_1) and second half (T_2) of the 10 min test (Repeated measures (RM) two-way ANOVA; time × drug × virus interaction $F_{1,54} = 4.48$, $p = 0.039$; main effect virus $F_{1,54} = 4.99$, $p = 0.030$ followed by RM ANOVA within subjects. Main effect time: scrShank3 vehicle: $F_{1,15} = 1.36$; shShank3 vehicle: $F_{1,12} = 7.87$; scrShank3 Ro: $F_{1,12} = 0.26$; shShank3

Ro: $F_{1,15} = 0.03$). **(d)** Bar graph of social preference during T_2, over the total social preference (Normalized SP2) (two-way ANOVA; virus × drug interaction: $F_{1,54} = 5.98$, $p = 0.018$; main effect virus: $F_{1,54} = 1.73$, $p = 0.194$; main effect drug: $F_{1,54} = 0.03$, $p = 0.875$; followed by Tukey HSD post-hoc test). **(e)** Time of social interaction during T_2 (two-way ANOVA; virus × drug interaction: $F_{1,54} = 1.07$, $p = 0.305$; main effect virus: $F_{1,54} = 3.84$, $p = 0.055$; main effect drug: $F_{1,54} = 0.27$, $p = 0.606$; followed by Tukey HSD post-hoc test). **(f)** Number of entries during T_2 (two-way ANOVA; virus × drug interaction: $F_{1,54} = 6.76$, $p = 0.012$; main effect virus: $F_{1,54} = 0.60$, p = 0.442; main effect drug: $F_{1,54} = 1.83$, $p = 0.182$; followed by Tukey HSD post-hoc test). The numbers indicate mice.

Europe PMC Funders Author Manuscripts

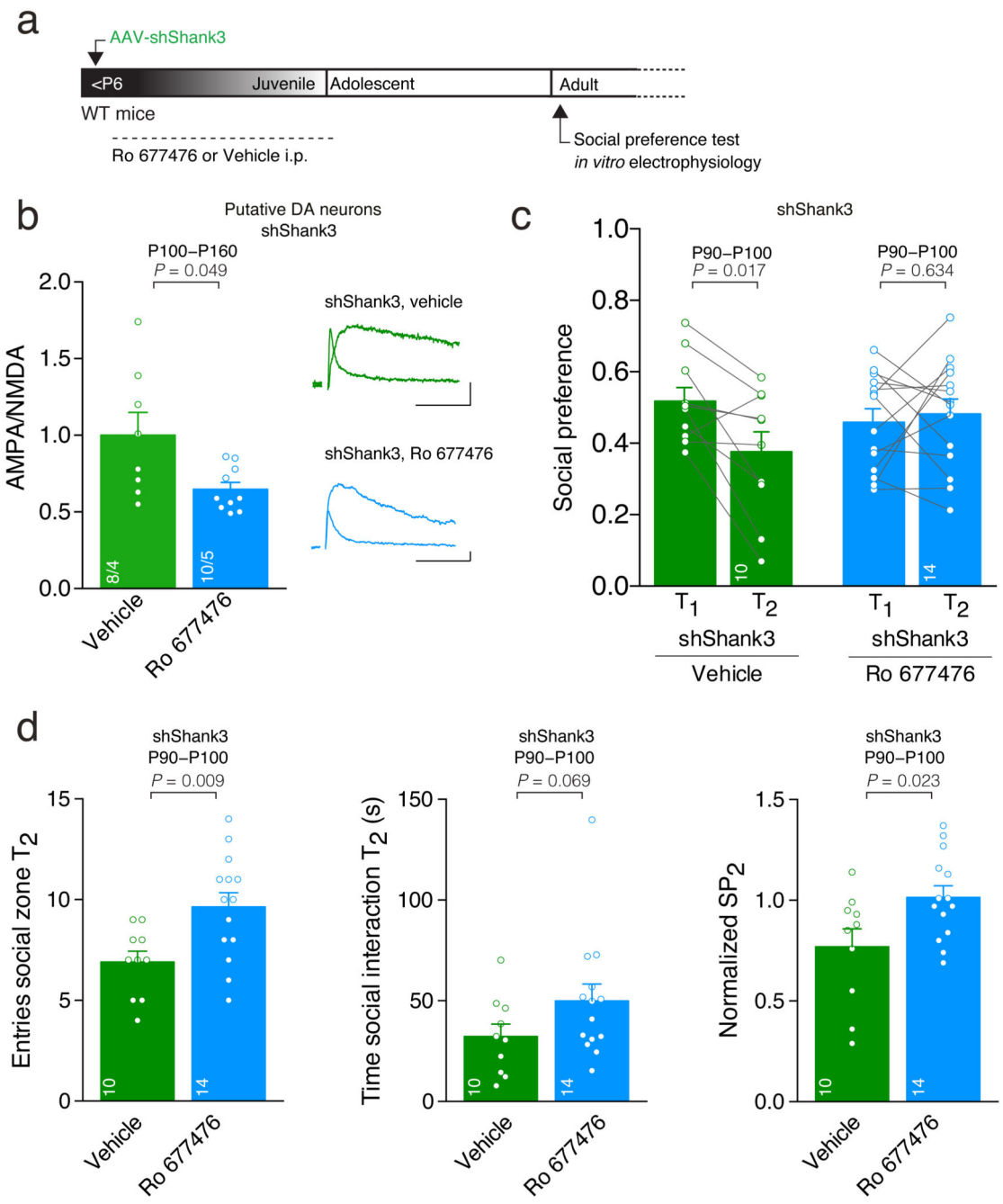

Fig. 7. Synaptic and social deficits persist into adulthood and are reversed by treatment with PAM-mGluR1 during the critical period.

(a) Experiment schematic. **(b)** Top: example traces of evoked AMPAR- and NMDAR-EPSCs recorded at +40 mV. Group mean AMPA/NMDA ratio calculated in shShank3 infected mice injected with vehicle or mGluR1-PAM Ro 677476 ($t_{8.33}$ = 2.30, unpaired t-test). The numbers indicate cells and mice. Scale bar: 20pA, 20ms. **(c)** Scatter plots and group mean representing the social preference during T_1 and T_2 (RM ANOVA; time × group interaction: $F_{1,22}$ = 5.56, p = 0.028, main effect group $F_{1,22}$ = 0.22, p = 0.644 followed by

Europe PMC Funders Author Manuscripts

RM ANOVA within subjects. Main effect time: shShank3 vehicle: $F_{1,9}$ = 8.58; shShank3 Ro: $F_{1,13}$ = 0.24). **(d)** Group mean entries around the social enclosure, time spent sniffing the stimulus mouse during T_2 and normalized social preference at T_2 for shShank3 mice treated with vehicle or Ro 677476 (entries: t_{22} = -2.88, unpaired t-test; time: U = 39.00, Mann-Whitney test; Normalized SP_2: t_{22} = - 2.44, unpaired t-test). The numbers indicate mice. Error bars show SEM.

Europe PMC Funders Author Manuscripts

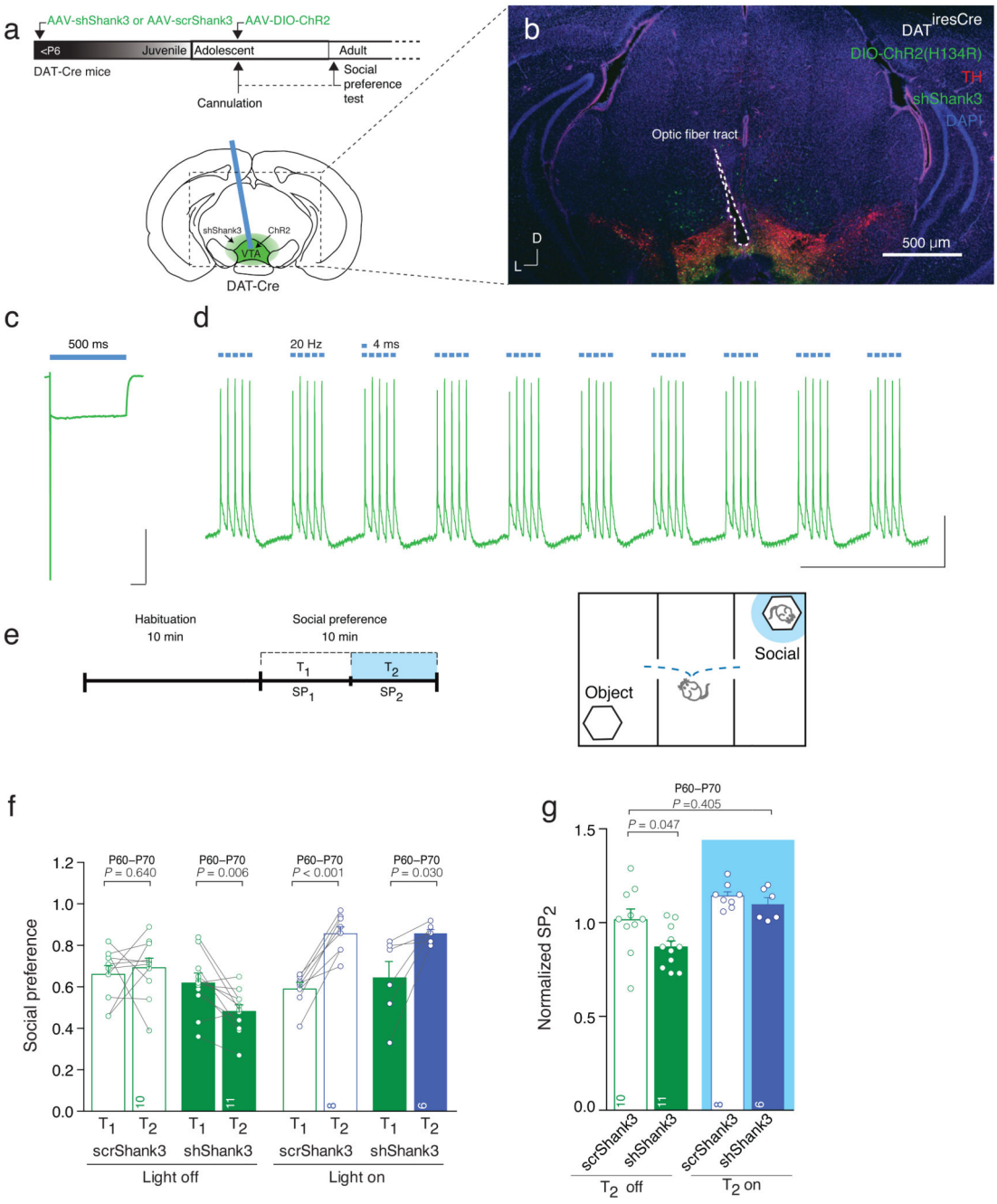

Fig. 8. Optical stimulation of VTA DA neurons increases social preference.

(a) Schematic of the experimental design, injection site and cannula placement. **(b)** Representative image of cannula placement and injection site of the AAV-shShank3 and AAV-DIO-ChR2 in the VTA. Scale bar: 500µm. **(c)** Whole cell patch clamp recording of ChR2 infected VTA DA neuron, showing desensitizing photocurrent in response to 500 ms blue light. Scale bar: 100 ms, 1nA. (**d**) *In vitro* validation of 20 Hz blue light stimulation protocol. Scale bar: 1 s, 10mV. **(e)** Experiment schematic. Optical stimulation was applied during the second 5 min of the test (T_2), only when animals were in proximity to the

Europe PMC Funders Author Manuscripts

Europe PMC Funders Author Manuscripts

enclosure containing the stimulus mouse. **(f)** Scatter plots and group mean of social preference for each condition (Repeated measures (RM) two-way ANOVA; time × drug × virus interaction $F_{1,31} = 1.11$, $p = 0.300$; light stimulation × virus interaction $F_{1,31} = 5.52$, $p = 0.025$; main effect virus $F_{1,31} = 2.28$, $p = 0.141$; main effect of light stimulation $F_{1,31} = 14.17$, $p = 0.001$; followed by RM ANOVA within subjects. Main effect time: scrShank3 off: $F_{1,9} = 0.23$; shShank3 off: $F_{1,10} = 11.77$; scrShank3 on: $F_{1,7} = 55.14$; shShank3 on: $F_{1,5} = 9.03$). **(g)** Group mean normalized social preference SP_2 (two-way ANOVA; virus × light stimulation interaction: $F_{1,31} = 1.28$, $p = 0.267$; main effect virus: $F_{1,31} = 4.70$, $p = 0.038$; main effect light stimulation: $F_{1,31} = 16.93$, $p < 0.001$; followed by Dunnett post-hoc test). The numbers indicate mice.